

Excitonic superlens with copper and copper oxideDavid Ziemkiewicz^{✉,*}, Karol Karpiński, and Sylwia Zielińska-Raczyńska[✉]*Institute of Mathematics and Physics, Technical University of Bydgoszcz, Al. Prof. S. Kaliskiego 7, 85-789 Bydgoszcz, Poland*

(Received 21 May 2023; revised 31 July 2023; accepted 24 August 2023; published 31 August 2023; corrected 6 March 2025)

We investigate the imaging properties of copper-based superlens surrounded by copper oxide (Cu_2O). A subwavelength image resolution of the order $\lambda/9$ is demonstrated theoretically and verified in numerical simulations. It is shown that the existence of excitons in Cu_2O influences the static and dynamical optical properties of the lens, providing an unique way of optically controlling the lens properties. In particular, an improvement of image quality caused by absorption in the spectral region of excitonic resonances is investigated. The plasmon-exciton interaction in the system may pave the way to tunable, highly nonlinear superlens designs.

DOI: [10.1103/PhysRevB.108.075307](https://doi.org/10.1103/PhysRevB.108.075307)**I. INTRODUCTION**

In recent years, subwavelength imaging and photolithography facilitated by metallic nanostructures has attracted significant attention [1]. Subwavelength imaging techniques originate from the concept of metamaterial superlens, introduced by Veselago in 1968 [2]. However, it has remained a theoretical possibility until 2000, when first negative index metamaterials have been constructed. Soon after, Pendry has demonstrated that such a lens is capable of imaging beyond diffraction limit [3] and that a simpler, metallic structure characterized only by negative permittivity can also work as a superlens under certain conditions. Since then, this field has become an important research topic. Noble metal nanostructures based on gold and silver have allowed the light to be guides beyond the diffraction limit, which has opened new possibilities for further miniaturization and applications of optoelectronic devices.

In 2005 Lee *et al.* [4] presented experimental and theoretical studies of the optical superlens using a thin silver slab and demonstrated optical imaging with resolution well below the diffraction limit. The investigations of different, cheaper material to construct efficient superlens systems basing on different metals have started; Zhao *et al.* [1] have studied several superlens materials, including Ni, Cr, and also Cu in the 400 nm wavelength range concluding that the dielectrics covering the superlens surfaces have to be characterized by similar permittivities, which influence the imaging quality. It has also been noted that a large permittivity of the dielectric in the front of the superlens is in favor of the imaging effect. Mkhitarian *et al.* have recently demonstrated that high- Q -factor plasmonic structures can be realized with copper [5], further confirming that Cu is a promising candidate for construction of efficient superlens.

The commonly used approaches to analysis of the metallic superlens are the transfer matrix and the numerical finite-difference in time-domain (FDTD) simulations [6]. They are

especially valuable in description of the detailed role of near-field optics in a superlens image formation, which has been reviewed recently by Adams *et al.* [7].

The important aspect of producing superlens is the accomplishment of the optimal resolution. It is affected by the finite thickness of the superlens, which generates both long- and short-range surface plasmon modes, they in turn influence a transfer function distorting the image field. Wang *et al.* [8] found that the presence of loss is not always detrimental to the superlens resolution, especially in the image side of the lens.

Since the discovery of negative index metamaterials and superlens, there is a strong need for a lens medium that is characterized not only by the necessary negative permittivity, but also one that offers tunability of its optical properties. By coupling various quantum systems with the metamaterial, one can provide such a capability [9]. These so-called quantum metamaterials [10] are a new class of media that bridges the gap between quantum systems and classical metamaterials. In this paper, we focus on the recently discovered Rydberg excitons (REs) in Cu_2O [11] and their potential application in copper based superlens. In particular, the possibility to control the properties of the lens by optically modulating the exciton density is explored. This is an unique feature facilitated by specific properties of Cu and Cu_2O that allow for efficient plasmon-exciton interaction [12].

Exciton is a highly excited electron-hole pair bound by Coulomb attraction, forming a solid-state analog of hydrogen atom [13]. The first theoretical description of excitons has been provided by Frenkel [14] and expanded by Wannier and Mott [15,16]. In this paper, we focus on Wannier-Mott type excitons that occur in Cu_2O , which was one of the first semiconductors where excitons have been observed [17]. Due to the possibility of creating P-type envelope wave-function excitons characterized by a principal quantum number $n \gg 1$, they have been called Rydberg excitons, in analogy to Rydberg atoms.

In principle, various properties of RE have a similar scaling with principal quantum number n as Rydberg atoms [18] although the physical origin of these similarities in their case

*david.ziemkiewicz@utp.edu.pl

TABLE I. Parameters of Cu fitted in Drude-Lorentz model to experimental [26]. The Cu₂O fitted to bulk experimental data [11], considering only 2P-exciton.

Medium	ϵ_∞	f_0 [eV ²]	ω_0 [eV]	Γ_0 [eV]	f_1 [eV ²]	ω_1 [eV]	Γ_1 [eV]
Cu ₂ O	7.5	489×10^{-7}	2.147	0.0049	0	0	0
Cu	15.3	122.18	0	0.0025	3.18	2.37	0.20

bases on a complex valence band structure and different selection rules for excitons. The dimensions of REs scale as n^2 and can reach micrometers, and their lifetimes are $\sim n^3$ and can reach hundreds of nanoseconds. Another exceptional feature is their strong interaction with external fields due to the fact that their polarizability scales as n^7 . Significant feature of Rydberg excitons is Rydberg blockade, which is a result of a long-range dipole-dipole and Van der Waals interactions between them that can be large enough to perturb the energy level of nearby excitons, so they no longer have the same frequency, which prevents their excitation in the immediate vicinity of already existing exciton. Nowadays REs become one of the rapidly developing topic in solid-state optics; the studies extend from linear to nonlinear regimes in bulk media and nanostructures [19–21]. Recently, REs interaction with plasmons has been studied, showing possibility of an evident extension of propagation length and bridging plasmonics and Rydberg excitons physics [12]. Here, we expand upon that work by considering the effect of excitons on the dynamics of copper-based superlens.

We perform a detailed analysis of Cu and Cu₂O, with its particularly high permittivity, taking into account all the above mentioned aspects. The required matching of permittivity of Cu and Cu₂O can be achieved either by tuning the frequency, adjusting the Cu film thickness [22] or using metal-dielectric composites [23] such as a fine mix of Cu and Cu₂O layers with excitons. Tailoring the optical properties of medium opened a new possibility of controlling the image. This is because the propagation dynamics of the field depends on the diffraction and dispersion properties of the medium. In particular, Archambault *et al.* [24] pointed out that an improvement of spatial resolution has to be achieved using time-dependent incident pulse. In the spirit of their conclusions we examine the influence of the group velocities of various modes on the image formation.

The paper is organized as follows. In the first section, a numerical model of the optical properties of copper and copper oxide is presented, which is later used in theoretical calculations and numerical simulations. Then, the system setup is outlined. The third section is devoted to the study of the steady-state transmission coefficient of the copper superlens. Next, the dynamic of the image formation in the superlens is investigated. Finally, the conclusions are presented. The detailed description of the numerical simulation method is included in the Appendix.

II. MATERIAL MODEL

For the numerical description of the optical properties of media considered in this paper, we use the Drude-Lorentz model in which the permittivity, in the case of two-oscillator

model, is given by [25]

$$\epsilon(\omega) = \epsilon_\infty + \frac{f_0}{\omega_0^2 - \omega^2 + i\omega\Gamma_0} + \frac{f_1}{\omega_1^2 - \omega^2 + i\omega\Gamma_1}, \quad (1)$$

with the numerical value of parameters summarized in Table I in the Appendix. In the case of Cu, the values of parameters are adjusted to provide a good fit to the experimental data presented in Ref. [26]. A comparison of the experimentally measured permittivity spectrum and the model values is shown in Fig. 1. The model is adjusted to provide a good fit in the energy region between $E \sim 2140$ – 2170 meV (dashed, vertical lines), where excitonic resonances are present. In particular, we assume that the optical properties of Cu are determined by an ensemble of free electrons. The oscillator strength f_0 is determined by density of electron plasma, with so-called plasma frequency $\omega_p = \sqrt{f_0} = \sqrt{Ne^2/m\epsilon_0}$, where N and m are the concentration of charges and effective mass of a single charge (electron). Due to the fact that the electrons are not bound, there is no restoring force that would result in some intrinsic resonant frequency of charges and so $\omega_0 = 0$. The damping parameter Γ_0 represents various dissipative processes. The parameters of the second oscillator f_1 , ω_1 , Γ_1 are used to include the effect of interband transitions that are responsible for an increase of absorption around 2.35 eV (see Fig. 1).

For the copper oxide, the same Eq. (1) with a different set of parameters can be used. The two main contributions to the Cu₂O susceptibility are the constant value of $\epsilon_\infty = 7.5$ and the effect of 2P exciton resonance, e.g., the exciton with hydrogen-like 2P orbital, characterized by quantum numbers $n = 2$, $l = 1$; this excitonic state is involved in the first and strongest radiative transition between valence band and excitonic levels [11]. Cu₂O is unique in this regard, since both

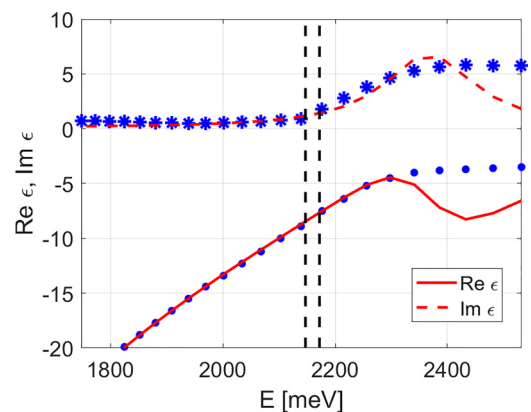


FIG. 1. Real (continuous line) and imaginary (dashed line) part of permittivity given by Eq. (1), compared to experimental data (dots).

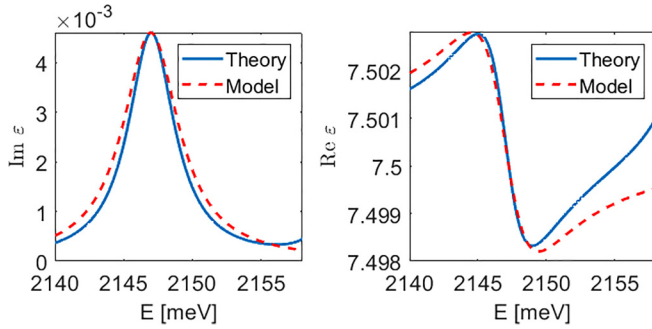


FIG. 2. Imaginary (left side) and real (right side) part of permittivity. Solid lines are given by theoretical calculation for Cu_2O bulk 2P exciton from Ref. [27] and dashed lines are given by Eq. (1) with parameters depicted in Table I.

valence and conduction bands have the same parity, which prevents electric dipole transition for excitons with S-type envelope wave functions, while excitons with P-envelope are dipole-allowed. Since the exciton oscillator strength scales as n^{-3} , as a first approximation we can ignore the states with $n > 2$. The permittivity described by such a model is shown in Fig. 2. The resonance is included as an oscillator with the frequency corresponding to the 2P exciton, with energy 2147 meV and the oscillator strength and damping constant adjusted to match the height and width of absorption peak of the exciton [27]. In particular, the maximum value of imaginary part of permittivity $\text{Im } \epsilon = 4.5 \times 10^{-3}$ corresponds to the absorption coefficient of $\alpha = \omega / (c\sqrt{\epsilon_b}) \sim 170 \text{ cm}^{-1}$, where ω is the frequency corresponding to 2147 meV; the obtained value is consistent with experimental observations [28]. In the case of Cu_2O , the second oscillator in Eq. (1) is unused. The model in Fig. 2 is valid under the assumption that the density of 2P excitons is uniform and limited only by the Rydberg blockade mechanism [11]. This is achieved by illuminating the system with external, uniform optical field (control field). By changing the field intensity, one can control the exciton density both spatially and temporally. In the case of Rydberg exciton states, the blockade volume of exciton becomes extremely large, so that even at low field intensity the system becomes saturated with excitons and absorption of light is reduced (so-called optical bleaching [11]). In such conditions, the optical properties of the system could be highly nonlinear. One can also see in Fig. 2 that the absolute value of the change of permittivity caused by excitonic resonance is relatively small, but it happens in a very narrow spectral range, which results in significant dispersion and thus modification of the group velocity.

The presented model of Cu permittivity yields the value of $\epsilon = -8.54$ at the bulk 2P exciton energy of 2147 meV, which is a 14% mismatch; however, as mentioned before, the metal permittivity depends on layer thickness [22]. Moreover, the optical properties of Cu_2O layers are also thickness dependent [29]; specifically, the gap energy, and thus also exciton energy can vary considerably. The permittivity of Cu_2O also depends on fabrication technique and layer thickness, reaching value of up to $\epsilon \sim 9$ [30,31]. We also note that a thin Cu_2O layer can be considered a confined system for excitons, increasing

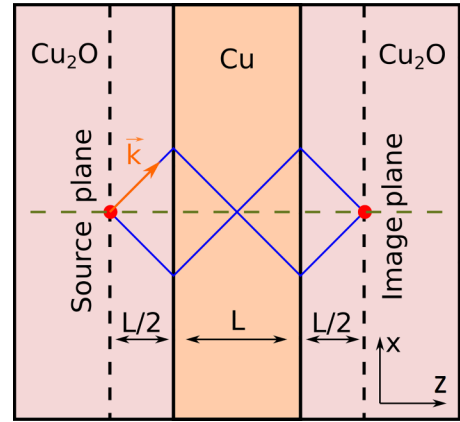


FIG. 3. Schematic representation of a copper superlens surrounded by Cu_2O .

their energy [32]. Finally, the permittivity mismatch can be in some cases beneficial to superlens imaging properties [33]. In conclusion, the fine optimization of the geometry and material properties is a complex issue beyond the scope of this manuscript.

III. SYSTEM SETUP

Let us consider a multilayer system consisting of a thin copper layer surrounded by copper oxide, as shown in Fig. 3. The optical axis of the system (horizontal, dashed line) is aligned to the z axis and the source/image planes (vertical dashed lines) are parallel to the x axis. We assume that the system is two-dimensional, e.g., it is much larger than wavelength in y axis and both material properties and fields do not change in that direction. Blue lines depict a schematic of optical rays connecting the line source (point on xz plane) with its image (red dots). For an efficient superlens operation, the thickness L needs to be considerably smaller than wavelength λ of the light illuminating the system [3], with approximate upper limit of 0.1λ [8]. To determine the superlens resolution, let us consider the wave vector k_0 and its x component k_x . Specifically, to achieve subwavelength resolution, the superlens needs to transmit high spatial frequency components with $k_x > k_0$. In such a case, the z component of the wave vector $k_z = \sqrt{k_0^2 - k_x^2}$ is imaginary and thus it describes evanescent waves. The key characteristic of the superlens is the capability to amplify these rapidly decaying evanescent waves [3].

IV. TRANSMISSION COEFFICIENT

One of the primary tools for studying the performance of the superlens is the transmission spectrum in the wave-vector domain, e.g., the relation $T(k_x)$. The system is capable of subwavelength imaging when the values of $T(k_x > k_0)$ are significant, indicating resonant amplification of evanescent waves, possibly beyond the amplitude of incident field. Similar to the approach presented in Ref. [8], we calculate the transmission coefficient (transfer function) of a flat superlens in electrostatic limit, e.g., in the case where the lens thickness is considerably smaller than illuminated wavelength. Let us consider a source and image plane located at a distance $L/2$

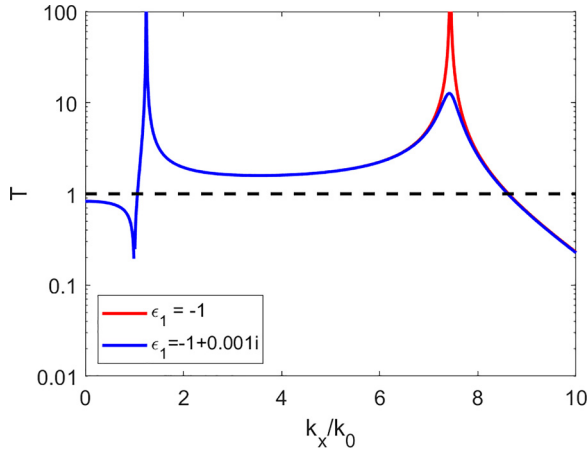


FIG. 4. Absolute value of the transmission coefficient as a function of the x component of wave vector k_x , calculated for a model superlens with $\epsilon = -1$.

from the superlens surfaces (see Fig. 3). Transmission coefficient is calculated by multilayer transmission using Parratt recursion relation [34], which applies standard Fresnel equations to compute reflection and transmission coefficient of a multilayer stack, accounting for reflection on each medium boundary and interference of reflected waves. Total amplitude transmission coefficient is given by

$$T = |T_0 T_1 \dots T_N|, \quad (2)$$

where T_j is the transmission coefficient in each layer, given by

$$T_j = e^{ik_z^{(j+1)}L_{j+1}} \frac{1 + F_j}{1 + F_j R_{j+1}}, \quad (3)$$

with reflection coefficient

$$R_j = e^{2ik_z^{(j)}L_j} \frac{F_j + R_{j+1}}{1 + F_j R_{j+1}}, \quad (4)$$

and

$$F_j = \frac{\epsilon_{j+1}k_z^j - \epsilon_j k_z^{j+1}}{\epsilon_{j+1}k_z^j + \epsilon_j k_z^{j+1}}. \quad (5)$$

The index $j = 0, 1, 2$ indicates the j th layer, counting from the source, correspondingly Cu_2O , Cu , and Cu_2O ; k_z^j is z component of wave vector in j layer and L_j is its thickness with $L_0 = L_{N+1} = 0$ and $R_{N+1} = 0$. Similar approach one can find in other papers about superlenses, see Refs. [35,36]. In this paper, we only consider the above-defined transmission coefficient that is a ratio of the near field amplitude in image and object plane, regardless of whether the field is propagating or evanescent. As pointed out in Ref. [36], by including the mechanism of coupling the image to the far field, one obtains a smaller transmission coefficient that is strictly limited to $T < 1$.

As a first step, we can verify the derived theoretical transmission relation by comparing it with the results presented by Wang *et al.* [8]. In particular, Fig. 4 depicts the absolute value of the transmission coefficient of idealized superlens consisting of a single layer of $\epsilon = -1$ material, with $\lambda/10$ thickness, surrounded by vacuum. There are several characteristic points in the transmission spectrum; for $k_x/k_0 < 1$, the

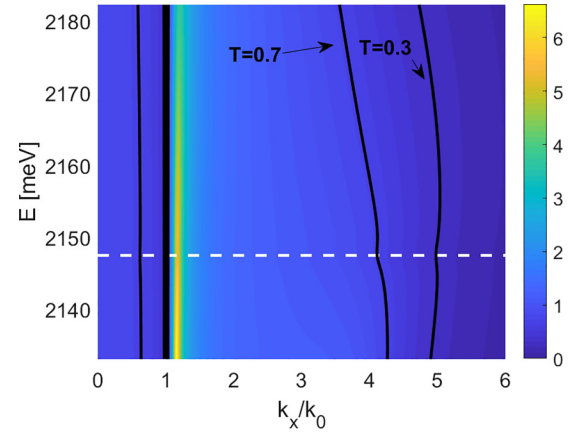


FIG. 5. Absolute value of the transmission coefficient (color) as a function of the x component of wave vector k_x and energy.

transmitted mode corresponds to regular, propagating wave; the transmission coefficient in this range is smaller than 1. For higher values of k_x , the transmission coefficient describes evanescent waves that do not carry energy since their Poynting vector has a zero real part, so one can have $T(k_x) > 1$. It should be stressed that $T(k_x) > 1$ only indicates that the field distribution forming the image contains local maxima that exceed the amplitude of incident field. This is related to the fact that plasmonic modes forming on the metal-dielectric boundary are slowly amplified over time until they reach the point where the power of ohmic losses in the metal match the incident power. For a system characterized with quality factor Q larger than 1, in such conditions the plasmon field can greatly exceed the incident field. Due to the presence of these resonant modes, the transmission spectrum usually contains two poles [8], which are clearly visible in Fig. 4. For $k_x/k_0 > 9$, there is a cutoff point where the transmission quickly drops. This means that the spatial resolution of the superlens is limited to approximately $\lambda/18$; one can increase this resolution by making the lens thinner [3]. The presence of the sharp poles in the transfer function (transmission coefficient) is generally undesirable as it introduces distortion [8]; one can see that the introduction of absorption (Fig. 4, blue line) significantly reduces the gain on the second, high k_x pole, so that the transfer function becomes more flat (e.g., all wave modes are amplified to a similar degree). Thus, despite the fact that absorption is in general detrimental to the superlens resolution, its presence can be beneficial to the image quality. Due to this reason, our proposal of Cu-based superlens has some advantages over traditional designs based on noble metals.

As a next step, we consider a copper superlens with a thickness $L = 20$ nm, surrounded by Cu_2O . From the perspective of practical applications, such a system is potentially simple to fabricate by controlled oxidation of Cu surface [37], vapor deposition [38], or other techniques [39]. The absolute value of the transmission coefficient calculated for a range of values of wave-vector component k_x and energy E is shown in Fig. 5. Due to the fact that copper has a significantly higher absorption coefficient than the idealized superlens material considered previously, there is only a single pole in the transmission coefficient at $k_x \approx k_0$. Overall, the usable range of

wave-vector values where transmission $T > 0.1$ is $k_x/k_0 < 6$, which corresponds to roughly $\lambda/12$ resolution and is comparable to silver superlens performance [40,41]. It should be stressed that this value is only a rough estimation of the resolution. Several techniques for evaluating and further improving the resolution exist [42]. One can notice that the strongest 2P exciton, which corresponds to 2147 meV (white, dashed line), produces a noticeable change in transmission coefficient (especially visible on the black contours). This means that the excitons in Cu_2O are a viable tool for fine-tuning of the lens properties in a very narrow energy range.

One of the primary considerations in the superlens design is the choice of thickness. In fact in the case of metallic lens with negative permittivity and positive permeability, the thickness needs to be much smaller than illuminated wavelength [43]. Also, in contrast to the ideal $n = -1$ superlens, there is a finite range of the values of wave-vector component k_x that are transmitted, as illustrated earlier in Fig. 5. In general, we can expect that high spatial frequency components of the image decay much faster in a thicker lens [8]. This is indeed the case in the calculated results shown in Fig. 6. Overall, there is a good match between theoretical and numerical results. The first local transmission maximum, which is also present in the idealized case in Fig. 4, forms a very sharp peak in theoretical calculations. To further confirm these results, we use the Finite-Difference Time-Domain (FDTD) simulation that is based directly on Maxwell's equations and thus allows for a direct study of superlens optical properties with no simplifying assumptions that are present in theoretical description. The only important limitation of FDTD is the limited time and spatial resolution, which results in a smaller, broader peak in the numerical transmission spectrum [Fig. 6(b)]. As mentioned before, the secondary peak in Fig. 4 located around $k_x = 7k_0$ is very sensitive to absorption and in case of Cu, it is almost completely suppressed. One can see that only in the case of $L = 12$ nm, a very wide local maximum of transmission is visible in Fig. 6 at $k_x \approx 5k_0$. Similar to the earlier results, the lack of sharp peaks in the transmission spectrum is beneficial, as it means that all spatial frequency components are amplified to the same degree [8]. In general, a lens thickness L of the order of 10 nm is favorable, with significant transmission up to $k_x/k_0 \approx 10$. As the lens becomes thicker, the transmission cutoff becomes smaller, up to $k_x/k_0 \approx 2$ for the thickest considered lens $L = 60$ nm. As noted in Ref. [44], the amplitude transfer function is only one of the metrics of superlens image quality; another one is phase transfer function, which describes how well the relative phase of various k_x modes is preserved. In particular, the phase $\phi(k_x)$ should be either unchanged [45] or, more realistically, change slowly with k_x , possibly in a linear manner [46,47]. To reconstruct image without distortions, the superlens needs to preserve the relative phase of various k_x modes. The phase transmission coefficient is shown in Fig. 6(c). In the case of the thinnest considered lens, the phase remains almost constant up to $k_x/k_0 \approx 5$, which is slightly smaller than the amplitude cutoff. This results in a resolution on the order of $\lambda/10$, which is consistent with FDTD simulations, where sources placed closer than $\lambda/10$ could not be distinguished. It should be mentioned that depending on the superlens purpose, either high-amplitude transfer, flat phase transfer function, or

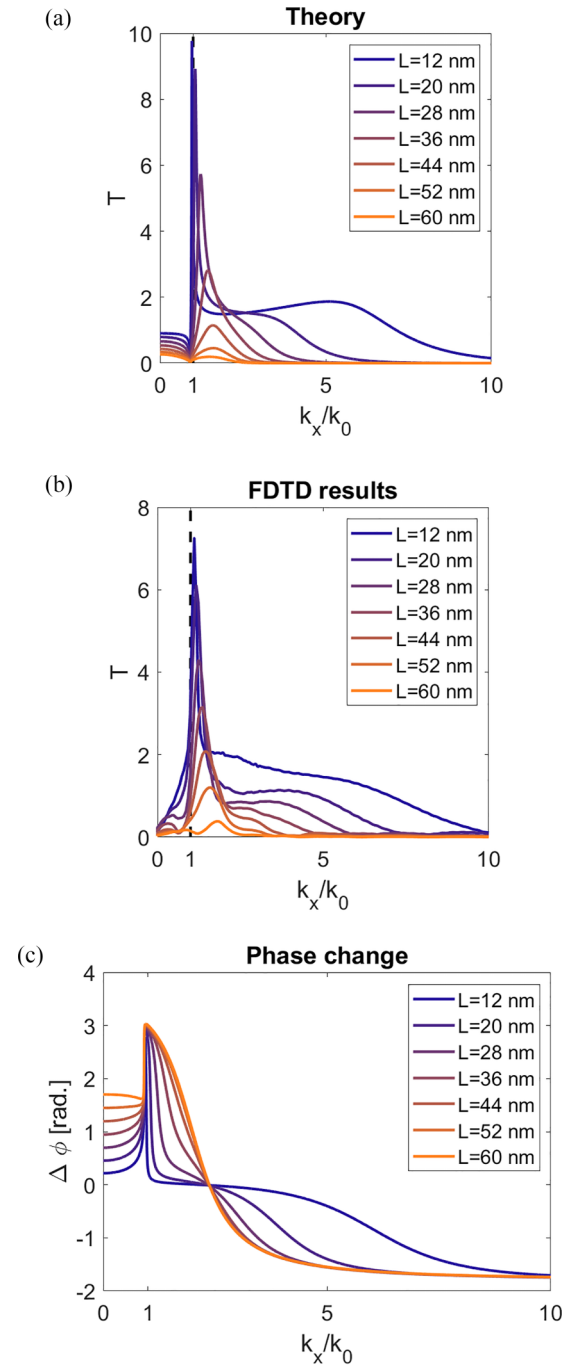


FIG. 6. Absolute value of the transmission coefficient as a function of the x component of wave vector k_x (a) calculated from Eq. (2) and (b) obtained in FDTD simulation; (c) phase of the transmitted waves.

suppression of spurious resonances can be the most important design factor [48].

After establishing the accuracy of the FDTD simulation, one can use the numerical results to investigate various aspects of superlens operation that are not described by the steady-state transmission coefficient. As mentioned in the discussion of Fig. 5, the presence of excitons has a limited impact on transmission coefficient; overall, the imaginary part of Cu_2O permittivity in the spectral range of 2P exciton resonance is of

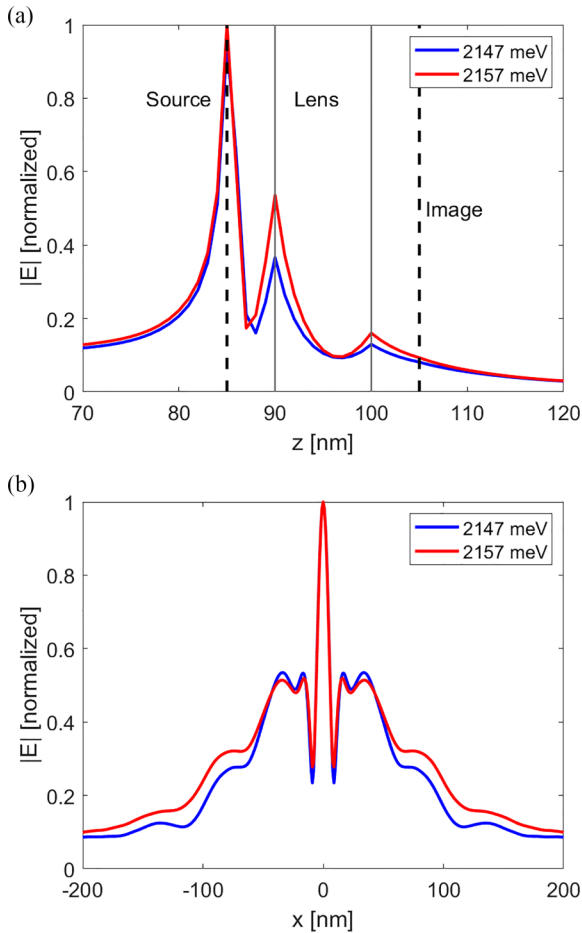


FIG. 7. Normalized total electric field amplitude (a) in the optical axis and (b) in the image plane.

the order of $\text{Im } \epsilon \sim 10^{-3}$ (Fig. 2) as compared to $\text{Im } \epsilon \sim 1$ in the case of copper (1). Therefore, the majority of absorption comes from the metal. However, it is well known that the surface plasmons-polaritons (SPPs) excited on the metal-dielectric interface are very sensitive to the susceptibility changes in the dielectric. In the case of superlens, these plasmons are excited on both metal-dielectric interfaces and they play a pivotal role in the evanescent field amplification and thus the image formation [3,49]. At the same time, they tend to distort the image field [8]. Therefore, the capability to fine-tune the absorption of dielectric surrounding the metallic lens with the use of excitons is potentially very valuable.

To study these plasmons and their influence on superlens operation, let us consider the numerically obtained electric field amplitude in the optical axis of the system, e.g., on the line connecting a single point source and its image, shown in Fig. 7(a). Naturally, the highest peak of the field amplitude is located at the source. One can also see significant peaks on the Cu-Cu₂O interfaces (continuous, vertical lines). These maxima correspond to surface plasmon resonances. Interestingly, the local maxima corresponding to SPPs are significantly affected by the presence of excitons. This means that the superlens containing excitons is capable of reconstructing the image while partially suppressing the surface plasmons. As a result, in the image of the point source [Fig. 7(b)],

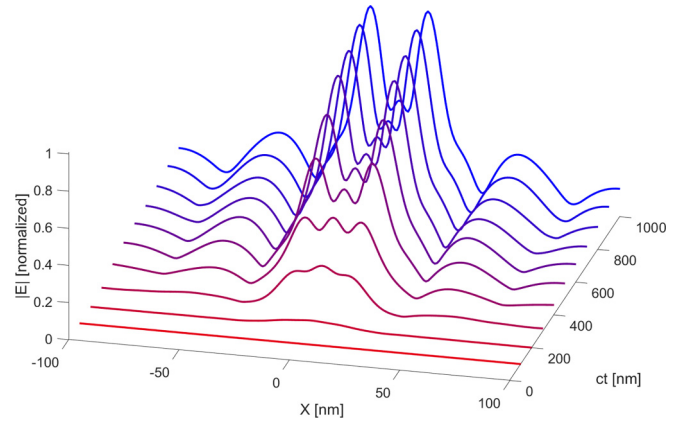


FIG. 8. Normalized field amplitude in the image plane as a function of time.

the side maxima caused by interference with the plasmons are reduced. These findings are consistent with the results by Wang *et al.* [8], where it is shown that adding loss in the image region can provide a significant enhancement of the image quality. In conclusion, we have demonstrated the improvement of superlens performance by the introduction of additional absorption due to excitons. Crucially, this absorption can be tuned by changing the exciton density with external field. It should be noted that the influence of excitons on the system is limited to a very narrow part of the spectrum; the largest 2P exciton resonance is characterized by a linewidth of $\Gamma \sim 5$ meV, while the energy range where a good match between Cu₂O and copper permittivity that allows for superlens operation is wider than the whole excitonic spectrum (see Fig. 1). This means that the system can be fine tuned with small changes of illuminating light frequency without impacting the image quality due to mismatch of permittivities.

V. SUPERLENS IN TIME DOMAIN

An important aspect of the comprehensive description of the superlens operation is the study of the time evolution of the image. Figure 8 depicts the field amplitude in the image plane of a $L = 20$ nm superlens illuminated by two point sources. The distance between sources is 40 nm, which is approximately $\lambda/5$ (the energy of 2147 meV corresponds to a wavelength of 571 nm in vacuum and 210 nm in Cu₂O). The time unit is scaled by the speed of light in Cu₂O which is around 1.1×10^8 m/s. One can see that initial, wide peak forming in the center of the image quickly transforms into two narrow peaks that are images of the radiation sources. The gradual formation of the image is caused by the varying group velocity of specific wave modes. In particular, the high k_x modes that correspond to the fine details of the image are characterized by a low group velocity and thus need longer time to propagate through the lens. Alternatively, one can describe this process in terms of mode amplification; an evanescent wave with very large k_x (e.g., large, imaginary wave vector) decays very rapidly in free space. Thus, to reconstruct the image, these modes need to be more amplified by the lens, which takes longer time.

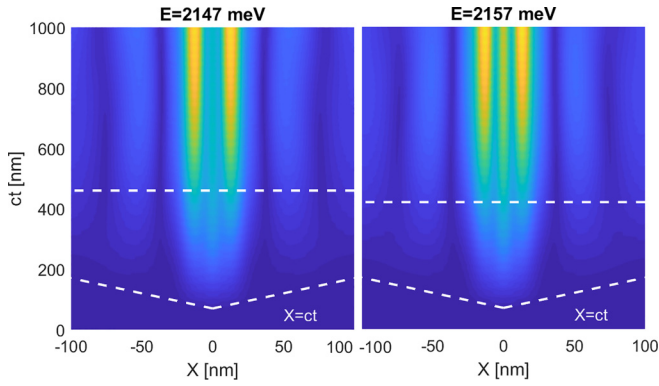


FIG. 9. Normalized field amplitude in the image plane (color) as a function of time, for two different energies.

In Fig. 9, a similar evolution is presented, calculated for two energies. On the left panel the energy is set to match the 2P exciton energy, while the right panel corresponds to the spectral region away from excitonic resonances. The diagonal dashed lines on the bottom correspond to the causality limit; no field can propagate in the system faster than $x = ct$. The horizontal dashed line corresponds to the moment when the image field reaches half of its maximum amplitude. In the case where excitonic resonance is present, the group velocity of wave modes is reduced due to the fact that an excitonic resonance corresponds to a sudden increase of normal dispersion. Specifically, we recall that the group velocity is given by

$$V_g = \frac{c}{n + \omega \frac{\partial n}{\partial \omega}}, \quad (6)$$

where ω is the radiation frequency and $n = \sqrt{\epsilon}$ is the refractive coefficient. In the spectral range of excitonic resonance, the permittivity changes very rapidly with frequency, so that $\partial n / \partial \omega$ has a significant value and noticeably reduces the group velocity [12]. Due to this, the image formation on the left panel of Fig. 9 is slightly delayed. Notably, the presence of excitons has a stabilizing effect on the image; the spurious peak located between the two source images is noticeably weaker in the left panel, confirming the earlier findings that additional absorption in dielectric is beneficial to the image quality.

It should be noted that the superlens resolution can be potentially greatly improved by considering time-dependent illumination [24]. The use of excitons opens up a new opportunity to provide time-dependent superlens properties; by using a separate control field, one can take advantage of the nonlinear properties of excitons in Cu_2O due to the Rydberg blockade effect and change its absorption on demand. In particular, the large blockade volume of Rydberg excitons with high principal quantum number can be especially valuable for such applications. Furthermore, the narrow resonances of high excitonic states result in a steep normal dispersion and greatly reduced group velocity. This, in turn, affects the propagation time of specific wave modes through the superlens, with slower modes also being more absorbed by the metal [12]. Finally, we recall that the optical properties of excitons are highly nonlinear [20]; in the case of superlens, the optical field is highly focused in subwavelength volume, further

enhancing the system nonlinearity, especially in high-power pulsed operation and higher excitonic states.

Another interesting possibility is the use an external field to modulate the spatial distribution of excitons and thus induce a spatially nonuniform optical properties of Cu_2O . In such a case, it might be possible to realize enhanced transmission of evanescent waves and improvement of resolution that are usually accomplished with lens surface roughness [8,43]. In contrast with fabricated roughness, the exciton distribution can be tuned on demand. Moreover, the spatial control of excitons and introduction of energy to the system via external field can be used as a loss compensation mechanism [50,51], enhancing the resolution. Finally, we note that spatial control of the optical properties of the Cu_2O layer can be also taken advantage of in far-field superlens designs [52], overcoming the main disadvantage of standard superlens that reconstructs the image only in the near field.

VI. CONCLUSIONS

Since their recent discovery in 2014, Rydberg excitons in Cu_2O have become a very valuable tool in creating nonlinear, controllable optical nanostructures. One of their possible applications are tunable plasmonic devices, where copper is used as the metal that facilitates excitation of SPPs and allows for easy fabrication of the structure. We show that a Cu layer surrounded by Cu_2O can act as an efficient superlens. It is demonstrated that such a device is capable of subwavelength imaging with a resolution approaching $\lambda/10$, which is competitive with traditional silver and gold based setups. Moreover, it is shown that excitons in Cu_2O can be used to modify the optical properties of the lens on demand and that the increased absorption due to the excitonic resonances is beneficial to the image quality. Several possible prospects for taking advantage of nonlinear optical properties of Cu_2O due to the excitons are outlined in the context of superlens design.

ACKNOWLEDGMENT

Support from the National Science Centre, Poland (NCN), project Miniatura, 2022/06/X/ST3/01162, is acknowledged.

The authors declare no conflicts of interest.

APPENDIX: FDTD METHOD

The performed simulations are based on a standard Yee algorithm [53], where a set of field evolution equations is derived from Maxwell's equations and used to update the electric/magnetic field values within some defined volume (computation domain), with a fixed time step. The whole domain is divided by a rectangular grid with a single cell size Δx . A two-dimensional system with TM field configuration is chosen for simplification of calculation; the electric field has two components in the plane of the propagation $\vec{E} = [E_x, 0, E_z]$, and the magnetic field has a single component perpendicular to the xz plane $\vec{H} = [0, H_y, 0]$. The two-dimensional representation is valid as long as the represented system (Fig. 3) is much larger than the wavelength in the y direction. At every grid point, the electric and magnetic field distributions are calculated from their previous values

with evolution equations derived directly from Maxwell's equations.

To model the dispersive properties of the optical media in the simulation, the auxiliary differential equation (ADE) approach is used [25]. The medium is characterized by a polarization vector $\vec{P} = [P_x, 0, P_z]$. The evolution of polarization is described by a second-order partial differential equation in the form

$$\ddot{\vec{P}} + \Gamma_j \dot{\vec{P}} + \omega_j^2 \vec{P} = \frac{\epsilon_0 f_j}{\epsilon_\infty} \vec{E}, \quad (\text{A1})$$

where ϵ_0 is vacuum permittivity, ϵ_∞ is the constant (frequency independent) part of permittivity and depending on the medium complexity, several oscillatory terms $j = 1, 2, 3, \dots$ can be used with fitted parameters f_j, Γ_j, ω_j . The full set of equations solved in our FDTD approach is as follows:

$$\frac{\partial H_y}{\partial t} = \frac{1}{\mu_0} \left(\frac{\partial E_x}{\partial z} - \frac{\partial E_z}{\partial x} \right), \quad (\text{A2})$$

$$\frac{\partial E_x}{\partial t} = \frac{1}{\epsilon_0} \left(\frac{\partial H_y}{\partial z} - \frac{\partial P_x}{\partial t} + j_x \right), \quad (\text{A3})$$

$$\frac{\partial E_z}{\partial t} = \frac{1}{\epsilon_0} \left(\frac{\partial E_x}{\partial z} - \frac{\partial P_z}{\partial t} + j_z \right), \quad (\text{A4})$$

where μ_0, ϵ_0 are the vacuum permittivity and permeability, respectively, and j_x, j_z are components of source current density. The above equations are rearranged to obtain time derivatives of the E_x, E_z, H_y fields, which are then used to calculate the field evolution with some constant time step Δt . Unit normalization is used so that $\mu_0 = \epsilon_0 = c = 1$. The parameters of Drude-Lorentz model of copper and copper dioxide, which are used in simulation are shown in Table I.

The simulation space is divided into a 300×1024 grid points. Computation domain is surrounded by absorbing

boundaries to reduce reflections. The spacial cell size $\Delta x = 4\text{nm}$ and time step $\Delta t = 6.67 \times 10^{-18}$ s. The total simulation time is on the order of 10^{-14} s which is sufficient for the surface plasmons excited on the lens boundaries to reach steady-state amplitude. At the same time, the optical properties of excitons are effectively static on this timescale (e.g., exciton density is constant, excitons are not moving, there is no exciton formation/recombination during the simulation). The lens system is placed in the middle of domain with optical axis in the x direction. A line source of radiation placed in source plane as a current j_x with sinusoidal time dependence. Such an infinite line of radiating dipoles, producing cylindrical, monochromatic waves with maximum amplitude in the z axis. We use a continuous radiation source with an amplitude that is adiabatically increased from 0 to its final value to avoid introducing high-frequency noise. Measurements are made after the amplitude reaches its full value and the field propagates through the lens. In the calculation of reflectivity spectrum, the field amplitude distribution in the object and image planes (Fig. 3) is calculated after steady-state operation is established. Then, a Fourier transform is performed to obtain the field distribution as a function of the wave-vector component k_x .

With the chosen time and spatial step, the image in the superlens starts forming after 2000 time steps and is fully formed after 8000 steps. The size of the simulation domain in the x direction is set to 1024 points to facilitate accurate fast Fourier transform in the spatial domain to obtain field distribution as a function of the wave-vector component k_x , and as a result the transmission coefficient. The field is averaged over time by using a moving average with a window size of 500 steps. In the image evolution analysis, a set of spatial field distributions is recorded at various times.

-
- [1] C. Zhao, Y. Zhou, Y. Zhang, and H. Wang, The imaging properties of the metal superlens, *Opt. Commun.* **368**, 180 (2016).
- [2] V. Veselago, The electrodynamics of substances with simultaneously negative values of ϵ and μ , *Sov. Phys. Usp.* **10**, 509-514 (1968).
- [3] J. B. Pendry, Negative Refraction Makes a Perfect Lens, *Phys. Rev. Lett.* **85**, 3966 (2000).
- [4] H. Lee, Y. Xiong, N. Fang, W. Srituravanich, S. Durant, M. Ambati, C. Sun, and X. Zhang, Realization of optical superlens imaging below the diffraction limit, *New J. Phys.* **7**, 255 (2005).
- [5] V. Mkhitarian, K. March, E. Tseng, X. Li, L. Scarabelli, L. Liz-Marzán, S. Chen, L. H. G. Tizei, O. Stéphan, J. Song, M. Kociak, F. Garcia de Abajo, and A. Gloter, Can copper nanostructures sustain high-quality plasmons? *Nano Lett.* **21**, 2444 (2021).
- [6] G. Tremblay and Y. Shen, Modeling and designing metallic superlens with metallic objects, *Opt. Express* **19**, 20634 (2011).
- [7] W. Adams, M. Sadatol, and D. O. Guney, Review of near-field optics and superlenses for sub-diffraction-limited nano-imaging, *API Advances* **6**, 100701 (2016).
- [8] H. Wang, J. Bagley, L. Tsang, S. Huang, K. Ding, and A. Ishimaru, Image enhancement for flat and rough film plasmon superlenses by adding loss, *J. Opt. Soc. Am. B* **28**, 2499 (2011).
- [9] J. Quach, C. Su, A. Martin, A. Greentree, and L. Hollenberg, Reconfigurable quantum metamaterials, *Opt. Express* **19**, 11018 (2011).
- [10] T. Stav, A. Faerman, E. Maguid, D. Oren, V. Kleiner, E. Hasman, and M. Segev, Quantum entanglement of the spin and orbital angular momentum of photons using metamaterials, *Science* **361**, 1101 (2018).
- [11] T. Kazimierzczuk, D. Fröhlich, S. Scheel, H. Stolz, and M. Bayer, Giant Rydberg excitons in cuprous oxide, *Nature (London)* **514**, 343 (2014).
- [12] D. Ziemkiewicz and S. Zielińska-Raczyńska, Copper plasmonics with excitons, *Phys. Rev. B* **106**, 205404 (2022).
- [13] R. S. Knox, *Theory of Excitons*, Solid State Physics Supplement (Academic Press, New York, NY, 1963).
- [14] Y. Frenkel, On the transformation of light into heat in solids, *Phys. Rev.* **37**, 17 (1931).
- [15] G. H. Wannier, The structure of electronic excitation levels in insulating crystals, *Phys. Rev.* **52**, 191 (1937).
- [16] N. F. Mott, Conduction in polar crystals. II. The conduction band and ultra-violet absorption of alkali-halide crystals, *Trans. Faraday Soc.* **34**, 500 (1938).
- [17] E. F. Gross and N. A. Karryjew, The optical spectrum of the exciton, *Doklady Akademii Nauk SSSR* **84**, 471 (1952).

- [18] J. Heckötter, M. Freitag, D. Fröhlich, M. Assmann, M. Bayer, M. A. Semina, and M. M. Glazov, Scaling laws of Rydberg excitons, *Phys. Rev. B* **96**, 125142 (2017).
- [19] K. Orfanakis, S. K. Rajendran, H. Ohadi, S. Zielinska-Raczynska, G. Czajkowski, K. Karpinski, and D. Ziemkiewicz, Quantum confined Rydberg excitons in Cu₂O nanoparticles, *Phys. Rev. B* **103**, 245426 (2021).
- [20] D. Ziemkiewicz, G. Czajkowski, K. Karpiński, and S. Zielinska-Raczynska, Nonlinear optical properties and Kerr nonlinearity of Rydberg excitons in Cu₂O quantum wells, *Phys. Rev. B* **106**, 085431 (2022).
- [21] C. Morin, J. Tignon, J. Mangeney, S. Dhillon, G. Czajkowski, K. Karpiński, S. Zielinska-Raczynska, D. Ziemkiewicz, and T. Boulter, Self-Kerr Effect Across the Yellow Rydberg Series of Excitons in Cu₂O, *Phys. Rev. Lett.* **129**, 137401 (2022).
- [22] O. Stenzel, S. Wilbrandt, S. Stempfhuber, D. Gäbler, and S. Wolleb, Spectrophotometric characterization of thin copper and gold films prepared by electron beam evaporation: Thickness dependence of the Drude damping parameter, *Coatings* **9**, 181 (2019).
- [23] W. Cai, D. A. Genov, and V. M. Shalaev, Superlens based on metal-dielectric composites, *Phys. Rev. B* **72**, 193101 (2005).
- [24] A. Archambault, M. Besbes, and J. J. Greffet, Superlens in the Time Domain, *Phys. Rev. Lett.* **109**, 097405 (2012).
- [25] N. Okada and J. B. Cole, Effective permittivity for FDTD calculation of plasmonic materials, *Micromachines* **3**, 168 (2012).
- [26] T. Hollstein, U. Kreibich, and F. Lens, Optical properties of Cu and Ag, *Phys. Status Solidi B* **82**, 545 (1977).
- [27] S. Zielinska-Raczynska, G. Czajkowski, and D. Ziemkiewicz, Optical properties of Rydberg excitons and polaritons, *Phys. Rev. B* **93**, 075206 (2016).
- [28] M. Aßmann and M. Bayer, Semiconductor Rydberg physics, *Adv. Quantum Technol.* **3**, 1900134 (2020).
- [29] A. Ait Hssi, L. Atourki, N. Labchir, M. Ouafi, K. Abouabassi, A. Elfanaoui, A. Ihlal, and K. Bouabid, Optical and dielectric properties of electrochemically deposited p-Cu₂O films, *Mater. Res. Express* **7**, 016424 (2020).
- [30] F. Haidu, M. Fronk, O. D. Gordan, C. Scarlat, G. Salvan, and D. R. T. Zahn, Dielectric function and magneto-optical Voigt constant of Cu₂O: A combined spectroscopic ellipsometry and polar magneto-optical Kerr spectroscopy study, *Phys. Rev. B* **84**, 195203 (2011).
- [31] C. Malerba, F. Biccari, C. L. A. Ricardo, M. D’Incau, P. Scardi, and A. Mittiga, Absorption coefficient of bulk and thin film Cu₂O, *Sol. Energy Mater. Sol. Cells* **95**, 2848 (2011).
- [32] D. Ziemkiewicz, K. Karpinski, G. Czajkowski, and S. Zielinska-Raczynska, Excitons in Cu₂O: From quantum dots to bulk crystals and additional boundary conditions for Rydberg exciton-polaritons, *Phys. Rev. B* **101**, 205202 (2020).
- [33] K. Lee, Y. Jung, G. Kang, H. Park, and K. Kim, Active phase control of a Ag near-field superlens via the index mismatch approach, *Appl. Phys. Lett.* **94**, 101113 (2009).
- [34] L. G. Parratt, Surface studies of solids by total reflection of x-rays, *Phys. Rev.* **95**, 359 (1954).
- [35] M. Splawinski, S. Bostock, K. J. Chau, and L. Markley, Superlens coupling to object and image: A secondary resonance mechanism to improve single-negative imaging of electromagnetic waves, *J. Appl. Phys.* **129**, 163102 (2021).
- [36] T. Hakkarainen, T. Setälä, and A. T. Friberg, Subwavelength electromagnetic near-field imaging of point dipole with metamaterial nanoslab, *J. Opt. Soc. Am. A* **26**, 2226 (2009).
- [37] O. Peña-Rodríguez and U. Pal, Effects of surface oxidation on the linear optical properties of Cu nanoparticles, *J. Opt. Soc. Am. B* **28**, 2735 (2011).
- [38] S. Steinhauer, M. A. M. Versteegh, S. Gyger, A. W. Elshaari, B. Kunert, A. Mysyrowicz, and V. Zwiller, Rydberg excitons in Cu₂O microcrystals grown on a silicon platform, *Commun. Mater.* **1**, 11 (2020).
- [39] S. A. Lynch, C. Hodges, S. Mandal, W. Langbein, R. P. Singh, L. A. P. Gallagher, J. D. Pritchett, D. Pizzey, J. P. Rogers, C. S. Adams, and M. P. A. Jones, Rydberg excitons in synthetic cuprous oxide Cu₂O, *Phys. Rev. Mater.* **5**, 084602 (2021).
- [40] G. Tremblay and Y. Sheng, Imaging performances of the metallic superlens, *Proc. SPIE* **7156**, 715602 (2009).
- [41] T. Hakkarainen, T. Setälä, and A. T. Friberg, Near-field imaging of point dipole with silver superlens, *Appl. Phys. B* **101**, 731 (2010).
- [42] A. Ghoshroy, W. Adams, and D. Ö. Güney, Theory of coherent active convolved illumination for superresolution enhancement, *J. Opt. Soc. Am. B* **37**, 2452 (2020).
- [43] N. Fang, Z. Liu, T. Yen, and X. Zhang, Regenerating evanescent waves from a silver superlens, *Opt. Express* **11**, 682 (2003).
- [44] C. P. Moore, M. D. Arnold, P. J. Bones, and R. J. Blaikie, Image fidelity for single-layer and multi-layer silver superlenses, *J. Opt. Soc. Am. A* **25**, 911 (2008).
- [45] M. Liu and C. Jin, Image quality deterioration due to phase fluctuation in layered superlens, *Optik* **121**, 1966 (2010).
- [46] S. Durant, Z. Liu, J. M. Steele, and X. Zhang, Theory of the transmission properties of an optical far-field superlens for imaging beyond the diffraction limit, *J. Opt. Soc. Am. B* **23**, 2383 (2006).
- [47] L. Yeh and J. Kiang, Multilayered superlenses containing CsBr or active medium for subwavelength photolithography, *Progr. Electromag. Res. B* **59**, 1 (2014).
- [48] C. P. Moore and R. J. Blaikie, Robust design of a silver-dielectric near-field superlens for photolithography, *J. Opt. Soc. Am. B* **30**, 3272 (2013).
- [49] D. R. Smith, D. Schurig, M. Rosenbluth, S. Schultz, S. Ramakrishna, and J. B. Pendry, Limitations on subdiffraction imaging with a negative refractive index slab, *Appl. Phys. Lett.* **82**, 1506 (2003).
- [50] A. Ghoshroy, W. Adams, X. Zhang, and D. O. Güney, Hyperbolic Metamaterial as a Tunable Near-Field Spatial Filter to Implement Active Plasmon-Injection Loss Compensation, *Phys. Rev. Appl.* **10**, 024018 (2018).
- [51] W. Adams, M. Sadatgol, X. Zhang, and D. Güney, Bringing the “perfect lens” into focus by near-perfect compensation of losses without gain media, *New J. Phys.* **18**, 125004 (2016).
- [52] Y. Xiong, Z. Liu, C. Sun, and X. Zhang, Two-dimensional imaging by far-field superlens at visible wavelengths, *Nano Lett.* **7**, 3360 (2007).
- [53] A. Taflove and S. Hagnes, *Computational Electrodynamics: The Finite-Difference Time-Domain Method*, 2nd ed. (Artech House, Norwood, MA, 2000).

Correction: The Acknowledgment section was missing and has been inserted.